



# Multi-million-year magmatic and hydrothermal activity is key to the formation of supergiant to behemothian porphyry copper deposits

Adrianna Luiza Virmond<sup>1</sup> · Jörn-Frederik Wotzlaw<sup>1</sup> · Rodrigo Rojas-Arancibia<sup>2</sup> · David Selby<sup>3</sup> · Cyril Chelle-Michou<sup>1</sup>

Received: 18 June 2024 / Accepted: 20 August 2024  
© The Author(s) 2024

## Abstract

Understanding the primary controls on mineral deposit formation and size is essential for sourcing the metals required by our ever-growing economy. The tonnage of porphyry copper deposits ranges five orders of magnitude but the key mechanisms and processes that modulate the size of these deposits remain enigmatic. Here, we investigate the behemothian deposits of the Chuquicamata Intrusive Complex (CIC) in northern Chile employing high-precision U–Pb and Re–Os geochronology. We resolve a complex long-lived magmatic-hydrothermal activity that lasted over 3.3 Myr. High-precision zircon petrochronology data indicate two distinct porphyry emplacement episodes, separated by 0.5 Myr, with the younger generation closely tied to the main intervals of hydrothermal mineralization. High-precision Re–Os molybdenite dates reveal a prolonged hydrothermal mineralization interval (> 2.5 Myr) that progressively migrated southwards within the CIC and continued after the end of the (apparent) magmatic activity. We show that the rate of copper precipitation varies little in nature (0.025–0.10 Mt/kyr) and is independent of the size of the deposit. Consistent with evidence from smaller deposits, our findings provide unprecedented evidence that copper endowment in porphyry copper deposits positively correlates with the timescales of magmatic and hydrothermal activity. Supergiant to behemothian deposits require multi-million-year magmatic-hydrothermal activity, linking the largest porphyry copper systems to a simple metric – the duration of magmatic-hydrothermal activity.

**Keywords** Porphyry copper systems · Timescales · Zircon · Molybdenite · Petrochronology · Chuquicamata

## Introduction

Global demographic and economic development in addition to the pursuit of alternative green sources of energy will significantly increase the demand for metals in the coming decades, pushing exploration geologists to find more economically viable deposits (Jowitt et al. 2020). Porphyry copper systems are the main source of copper and important

sources of other base metals and will continue to play a key role in future supply of these materials (Mudd et al. 2013). Even though these systems have been studied in detail and key ore-forming processes are well understood, one important question remains unanswered: what controls the tonnage of porphyry copper deposits (PCDs)?

The tonnage distribution of PCDs varies by over five orders of magnitude (Singer et al. 2008) with behemothian deposits (> 31.6 Mt of contained Cu, see Clark 1993) representing the largest end-member of this size distribution in nature. Some studies have suggested that such large-endowment PCDs are the result of the “perfect alignment” of geological processes (Richards 2013). Recent studies have applied numerical simulations to test these models and suggest that the volume and duration of the ore-forming magmatic-hydrothermal activity are the dominant controls in the total metal endowment of a deposit (e.g. Chelle-Michou et al. 2017; Chiaradia and Caricchi 2022). Such simulations agree with high-precision geochronological records of a

Communicated by Othmar Müntener.

✉ Adrianna Luiza Virmond  
adrianna.virmond@eaps.ethz.ch

<sup>1</sup> Institute of Geochemistry and Petrology, ETH Zurich, 8092 Zurich, Switzerland

<sup>2</sup> Gerencia de Planificación Distrital, CODELCO, Calama, Chile

<sup>3</sup> Department of Earth Sciences, University of Durham, Durham DH1 3LE, UK

handful of very large to supergiant (1–31.6 Mt Cu) deposits (e.g., Corocochuayco, Bajo de la Alumbrera, Bingham Canyon, Qulong, Batu Hijau). However, these available data cover only about one order of magnitude of Cu endowment making the extrapolation of the duration vs endowment relationship poorly constrained.

Determining the absolute timing and duration of upper crustal magmatic-hydrothermal processes requires geochronologic methods with absolute precision and accuracy on the order of a few thousand years (Annen 2009; Weis et al. 2012; Kent and Cooper 2017). For samples beyond the U–Th disequilibrium range (ca. > 300 ka, e.g. Guillong et al 2016), such timescales can only be resolved with high-precision and high-accuracy methods such as zircon chemical abrasion isotope dilution thermal ionization mass spectrometry (CA-ID-TIMS) U–Pb and molybdenite negative thermal ionization mass spectrometry (N-TIMS) Re–Os geochronology (Li et al. 2017 and references therein; Schoene and Baxter 2017; Chelle-Michou and Schaltegger 2023). Thermochronological methods are also frequently employed to determine the duration of hydrothermal events, particularly  $^{40}\text{Ar}/^{39}\text{Ar}$  dating of micas (sericite, muscovite and biotite), feldspars and hornblende (e.g. Arnott 2003; Maksaev et al. 2004; Deckart et al. 2013; Chiaradia et al. 2013). However, Ar diffusion (and consequent loss) in these mineral phases is temperature-sensitive making the isotopic system susceptible to resetting upon a heating event. Effectively,  $^{40}\text{Ar}/^{39}\text{Ar}$  Ar dates record the cooling below a mineral-specific temperature of Ar retention, potentially imposing challenges to the interpretation in long-lived complex settings (Chiaradia et al 2013). In addition, the  $^{40}\text{Ar}/^{39}\text{Ar}$  systems can suffer from excess  $^{40}\text{Ar}$  and  $^{39}\text{Ar}$  recoil which are particularly common in fine-grained material resulting in geologically meaningless dates (Harrison and McDougall 1981; Onstott et al. 1997; Baumgartner et al. 2009).

The Eocene–Oligocene Chuquicamata porphyry district in northern Chile ranks amongst the largest Cu accumulations in the world with over 190 Mt of contained Cu and a century-long mining history (Camus and Castelli 2021). Its geology has been extensively studied (e.g. Ossandón et al. 2001; Faunes et al. 2005; Rivera et al. 2012), providing an excellent framework to develop a high-precision geochronology study to constrain the processes and parameters that control the formation of behemothian PCDs. We investigate the timing and duration of magma emplacement and evolution and the timescales of hydrothermal activity in the Chuquicamata porphyry system employing high-precision zircon CA-ID-TIMS U–Pb and molybdenite N-TIMS Re–Os high-precision geochronology on samples covering the entire lithologic diversity of the system (Fig. 1). We show that the Chuquicamata Intrusive Complex (CIC) and associated deposits formed over a protracted period, with a long-lived magmatic and hydrothermal history, confirming

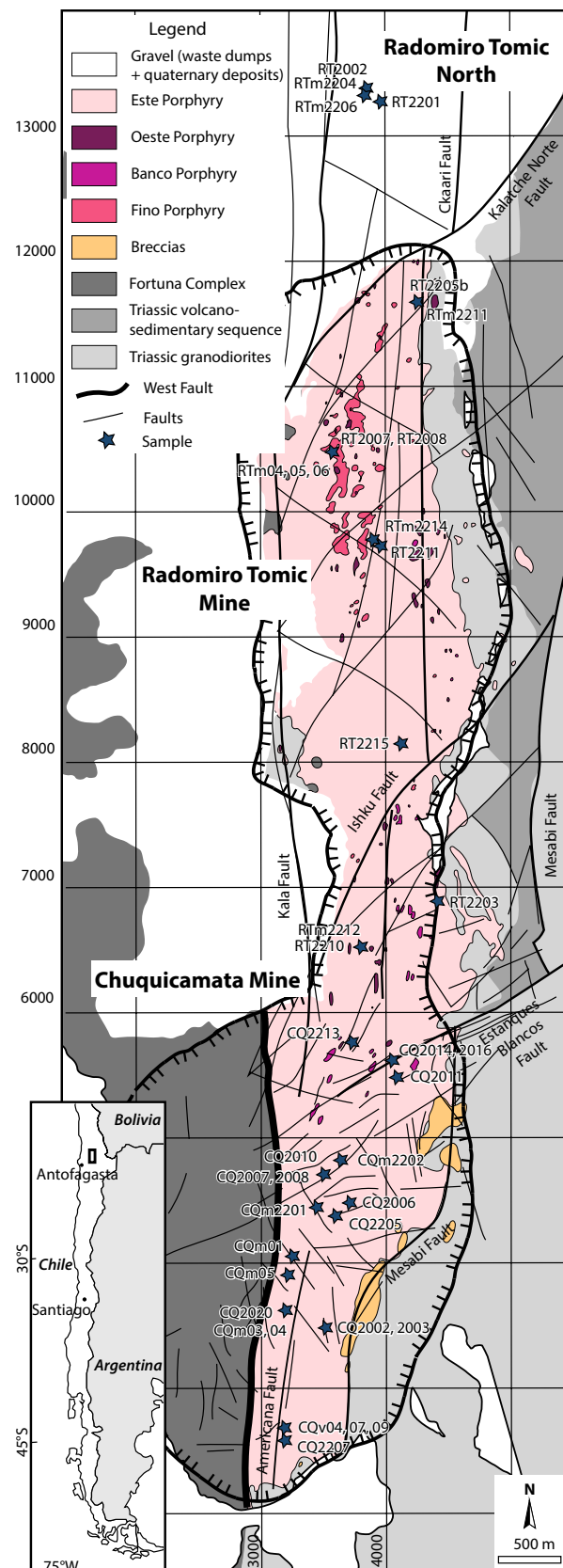


**Fig. 1** Updated geological map with outcropping units (based on the 2020 and 2023 CODELCO geological models) and modified after Tomlinson et al (2018)

numerical predictions that behemothian deposits form over million-year timescales. We also show that the average rate of copper precipitation in PCDs varies little (0.025–0.10 Mt/kyr) and that the timescale of hydrothermal activity has the greatest impact on the total endowment of a potential deposit.

## Geological setting

### Regional background

The tectonomagmatic evolution associated with the Eocene–Oligocene compressional phase of the Andean tectonic cycle is characterised by the formation of the Bolivian oroclinal bending, the eastward migration of the magmatic arc and the development of north–south trending parallel metallogenic belts extending from southern Peru to central Chile (Camus and Dilles 2001; Cobbold et al. 2007; Mamani et al. 2010). Located in northern Chile, the Domeyko fault system is a major tectonic structure that has been active since the late Eocene (Maksaev and Zentilli 1988, 1999; Camus and Dilles 2001; Amilibia et al. 2008) and has been viewed as a first order control on the emplacement of major Eocene porphyry systems in northern Chile, with some intrusions being emplaced syntectonically along faults (e.g. at Chuquicamata and La Escondida, Camus and Dilles 2001; Amilibia et al. 2008; Mpodozis and Cornejo 2012).

The Eocene–Oligocene metallogenic belt hosts many of the largest porphyry Cu deposits in the world, including the behemothian Chuquicamata district with almost 190 Mt of copper (combining past production and geological resources, Codelco 2022; Camus and Castelli 2021). The West Fissure (local name for the Domeyko fault system) divides the area into two blocks: the eastern, where the Chuquicamata, Radomiro Tomic and Mina Sur deposits are located; and the western block, hosting the Ministro Hales deposit, the Toki cluster deposits and the Los Picos and Fortuna igneous complexes (Ossandón et al. 2001; Rivera et al. 2012; Tomlinson et al. 2018).

### The Chuquicamata intrusive complex

The Chuquicamata Intrusive Complex (CIC; Tomlinson et al. 2018) comprises the Eocene–Oligocene intrusive rocks associated with the Cu–Mo mineralization at the Chuquicamata and Radomiro Tomic deposits. It occurs as an NNE 14 km-long, 0.7 to 2 km-wide west-dipping subvertical dike-like body that mostly crops out within the open pits (Rivera et al. 2012, Fig. 1). At Chuquicamata, the unit presents, to the east, both intrusive and faulted contacts with the Triassic East and Elena granodiorites and with the Jurassic meta-sedimentary rocks of the Caracoles Group (Tomlinson et al.

2018). To the west, it is truncated by the West Fissure, which juxtaposes the complex against the Eocene Fortuna Complex (Ossandón et al. 2001; Rivera et al. 2012; Tomlinson et al. 2018). Within the Radomiro Tomic mine, the complex presents intrusive contacts with the Elena granodiorite both to the east and to the west (Rivera et al. 2012).

Four main lithologies are recognized in the CIC, named Este (East), Oeste (West), Banco (Bench) and Fino (Fine) Porphyries, all of which possess varying degrees of hydrothermal alteration. The Este Porphyry unit is the most abundant lithology and hosts the other porphyries, which occur as small (metric to decametric) dike and stock-like bodies, preferentially in the central and northern parts of the CIC (Tomlinson et al. 2018). All porphyries share a similar granodioritic composition and mineralogy (plagioclase, quartz, alkali feldspar, biotite, titanite,  $\pm$  hornblende), and have a wide range of phenocrysts and groundmass proportion (e.g. Tomlinson et al. 2018, Fig. 2). The four porphyries are classified based on their distinct textural characteristics (e.g. Lindsay et al. 1995; Ossandón et al. 2001; Faunes et al. 2005; Rivera et al. 2012; Tomlinson et al. 2018). The Este porphyry presents lower groundmass proportion and coarser crystal size compared to the other porphyries. Banco differs from the Oeste porphyry by presenting bimodal distribution of plagioclase phenocrysts (one population ca. 0.5 mm long; one population typically > 2 mm long, Arnott 2003). The Fino porphyry presents finer granulometry (of groundmass and biotite crystals) compared to the Este porphyry (see Supplementary material for detailed descriptions).

While clear, sharp intrusive contacts have only been reported between the Este and Banco porphyries, other contacts between the Este and other porphyries have been variably described as diffuse and gradational (e.g., Oeste porphyries) or faulted (e.g., Fino porphyries; Ossandón et al. 2001; Faunes et al. 2005). Our observations have revealed intrusive contacts between the Este and all other porphyries (Fig. 2) and showed that the contact between the Oeste and Este porphyries can also be sheared.

All porphyries within the CIC have been hydrothermally altered and no clear spatial relationship between Cu grades and individual porphyry intrusions is observed (Ossandón et al. 2001; Faunes et al. 2005; Rivera et al. 2012; Skarmeta 2021). The distribution of alteration at Chuquicamata is zoned westward with a halo of propylitic alteration in the more distal part of the deposit, followed by a potassic zone that is gradually overprinted by main stage quartz–sericite, late quartz–sericite–pyrite and reaching advanced argillic alteration along the West Fissure, which truncates this zoning pattern (Ossandón et al. 2001; Faunes et al. 2005). At Radomiro Tomic, the same pattern of alteration styles is observed, but it develops symmetrically around the potassic core, and the argillic alteration is less pronounced (Rivera et al. 2012; Rojas-Arancibia 2023).



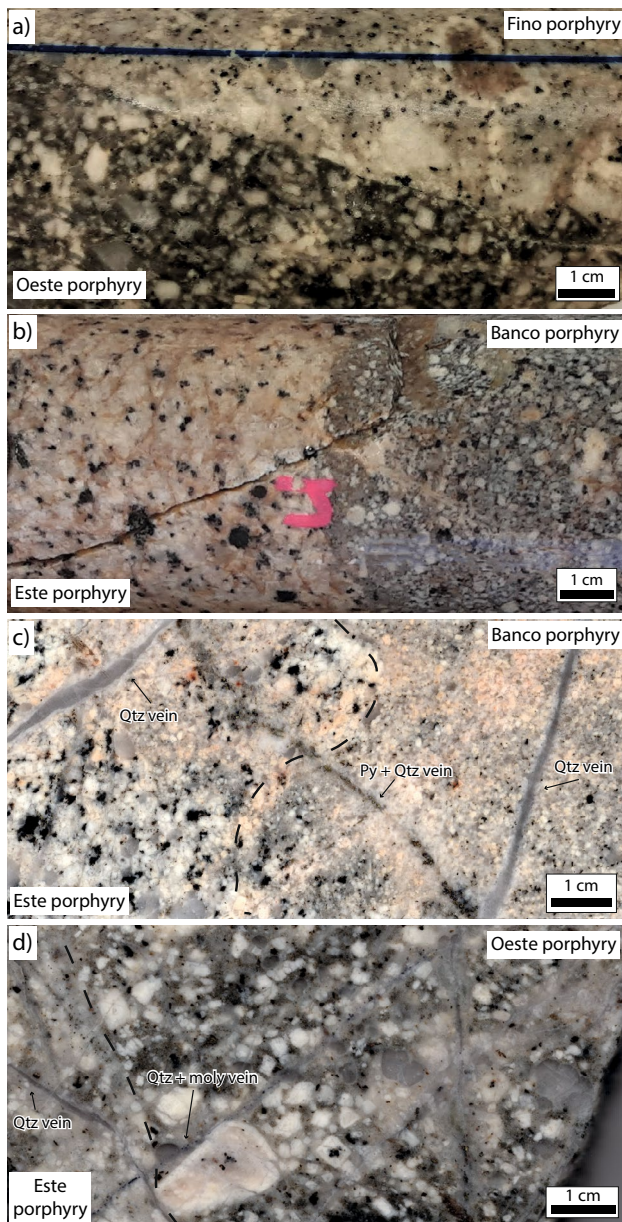


**Fig. 2** Different porphyry varieties and contact relationships for the CIC. **a** Contact between the Fino and Oeste porphyries in RT; **b** and **c** contact between the Banco and Este porphyries. Note the quartz (Qtz)+pyrite (Py) vein cuts the contact between porphyries; **d** contact between the Oeste and Este porphyries. Note the quartz-molybdenite (moly) vein cuts the contact between porphyries

Copper grades vary across the different alteration zones. In the rocks mostly affected by background potassic alteration, copper grades are low (0.2–0.5%), and mineralization is mostly disseminated or along fractures. However, within the zones of intense potassic and quartz-sericite alteration, Cu grades are typically 0.6 to 2 wt.% Cu (locally up to 5 to 10 wt.% Cu) representing most of the hypogene copper production in Chuquicamata (Faunes et al. 2005; Rivera

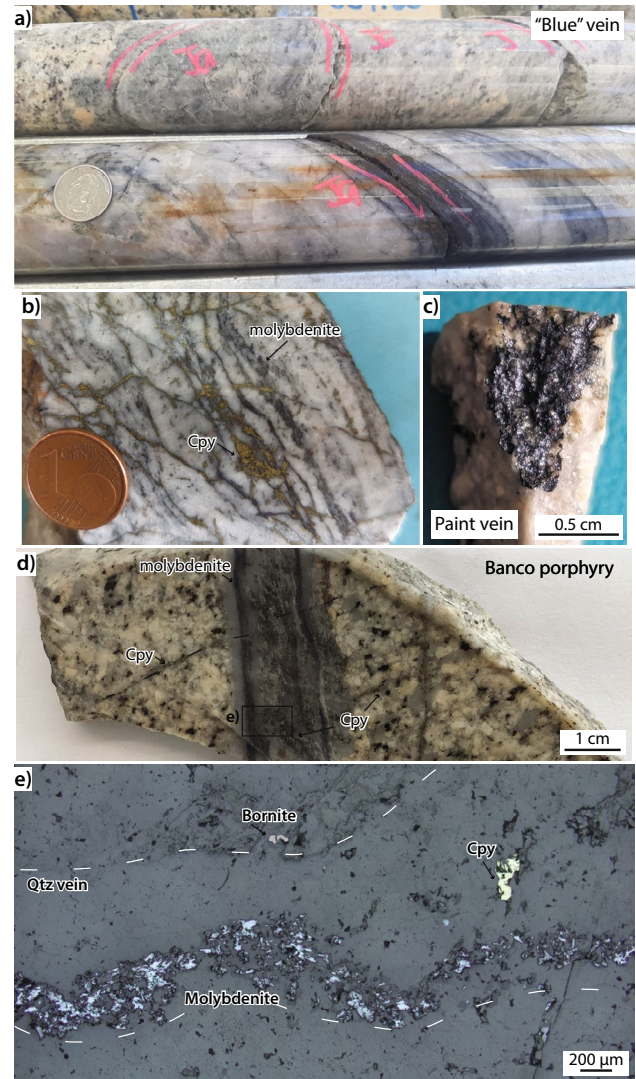


**Fig. 3** Molybdenite veins in the Chuquicamata Intrusive Complex. **a** Blue vein, coin for scale; **b** massive quartz-molybdenite vein cut by chalcopyrite (Cpy), coin for scale; **c** open paint vein; **d** re-opened quartz-molybdenite B vein, cut by chalcopyrite vein; **e** reflected light image of molybdenite in thin section, concentrated on the side of the vein

et al. 2012). Copper grades in the late quartz-sericite-pyrite zone appear to mimic those inherited from the overprinted intense potassic alteration with only minor upgrading of the Cu content (Faunes et al. 2005). The more distal propylitic altered rocks generally present low copper grades (<0.3%).

Early quartz and quartz-K feldspar veins (mostly A-veins) with minor Cu sulphides are cut by quartz-molybdenite veins (e.g. Fig. 2d). Molybdenite occurs mainly disseminated in centimetric B-veins, on larger (up to > 1 m wide) banded quartz-molybdenite veins often called blue veins (Ossandón et al. 2001; Rivera et al. 2012) and as “smears” in cracks, here referred to as paint veins (Fig. 3). While the distribution of the quartz-molybdenite mineralization follows that of the

main stage quartz-sericite and of the late-stage quartz-sericite-pyrite alteration, late quartz-sericite-pyrite veins clearly cut the molybdenite-bearing veins (e.g. Fig. 3d) and often form an alteration halo around them due to reopening of the previously existing veins (Ossandón et al. 2001; Rivera et al. 2012). In these reopened veins, molybdenite often occurs close to the borders (Fig. 3d, e). The relationships of the quartz-molybdenite mineralization to the main-stage copper event are less well-constrained but crosscutting relationships and the spatial distribution of the alteration and mineralization suggest that the molybdenite event dominantly predates the main stage copper introduction at any given location (Fig. 3; Ossandón et al. 2001; Faunes et al. 2005; Rivera et al. 2012; Skarmeta 2021). In the CIC, the molybdenite paint veins are often interpreted as remobilized Mo by later hydrothermal activity (Ossandón et al. 2001).

Previous geochronological studies conducted for the Chuquicamata district identify two ages of porphyry intrusion. The Este porphyry yielded zircon U–Pb SHRIMP age of  $35.2 \pm 0.4$  Ma while the Oeste and Banco porphyries yielded younger and indistinguishable crystallization ages ( $34.0 \pm 0.3$  and  $34.1 \pm 0.3$  Ma, respectively; Ballard et al. 2001). Additional ages (Campbell et al. 2006) of  $35.0 \pm 0.3$  (SHRIMP) and  $34.3 \pm 0.3$  (LA-ICP-MS) are also reported for the “major unit” in Radomiro Tomic (most likely the Este porphyry in RT) and of  $33.9 \pm 0.4$  Ma (LA-ICP-MS) for the “minor phase” in the mine (most likely the Fino Porphyry according to Rivera et al. 2012). An age of  $35.9 \pm 0.4$  Ma (U–Pb zircon, LA-ICP-MS) is reported for the Este porphyry in Radomiro Tomic (Tomlinson et al. 2018).

The timing of hydrothermal alteration in the CIC has been assessed with  $^{40}\text{Ar}/^{39}\text{Ar}$  dating of K-feldspar, biotite, muscovite and sericite (Reynolds et al. 1998; Arnott 2003; Barra et al. 2013). Muscovite/sericite dates range from  $30.6 \pm 0.3$  to  $32.1 \pm 0.3$  Ma, biotite dates range from  $31.1 \pm 0.2$  to  $33.6 \pm 0.5$  (except for 1 sample of chloritized biotite that yielded  $34.9 \pm 0.3$  Ma, Reynolds et al. 1998) and K-feldspar dates range from  $30.6 \pm 0.4$  to  $33.6 \pm 0.2$  Ma. Recent Re–Os molybdenite geochronology for the Chuquicamata mine include dates for B-type veins that constrain mineralization between  $32.9 \pm 0.2$  and  $31.9 \pm 0.2$  Ma (Barra et al. 2013), and for blue veins, with dates of  $31.7 \pm 0.3$  and  $32.2 \pm 0.3$  Ma (Zentilli et al. 2021). These Re–Os molybdenite dates suggest there is no temporal distinction between the two types of veins.

Despite the absence of cross-cutting evidence for syn- and post-mineralization porphyry intrusions, the long-lived protracted magmatic-hydrothermal history of Chuquicamata has led authors to suggest superimposed events that ultimately produced the gigantic deposit (e.g. Ballard et al. 2001) but the current geochronologic database does not provide enough precision (and as we will show, accuracy) to distinguish discrete events of magmatic or hydrothermal activity.

## Methods

### Samples and sample characterisation

Representative samples of all porphyries (Este, Oeste, Fino and Banco) were selected, covering a wide geographical distribution within the Chuquicamata Intrusive Complex (Fig. 1). Their modal mineralogical content was quantified through point counting on thin sections (see supplementary material). Zircon separates were obtained by applying crushing, panning, sieving and density separation with heavy liquid (methylene iodide). After handpicking, the grains were thermally annealed, mounted in epoxy, and polished. Cathodoluminescence (CL) images were obtained in a JEOL JSM-6390 LA scanning electron microscope (SEM) equipped with a Centaurus panchromatic CL detector. Trace element data and preliminary U–Pb dates were obtained by LA-ICP-MS at the Institute of Geochemistry and Petrology of ETH Zurich, using a 193 nm Resonetics Resolution S155 laser ablation system coupled to a Thermo Element XR sector-field single collector ICP-MS (Guillong et al. 2014). Details on instrument settings and data reduction are given in the supplementary material.

### High-precision U–Pb geochronology

Based on the LA-ICP-MS results, 10 to 15 previously dated grains from each sample were extracted from the mount and selected for high-precision geochronology using chemical abrasion isotope dilution thermal ionization mass spectrometry (CA-ID-TIMS). Analyses were conducted on a Thermo TRITON Plus thermal ionization mass spectrometer equipped with an axial secondary electron multiplier and faraday cups connected to  $10^{13} \Omega$  resistors in a setup similar to those described in von Quadt et al. (2016), Wotzlav et al. (2017) and Schaltegger et al. (2021). Further details on the analytical method and data reduction are presented in the supplementary material. All dates are reported with 2 sigma analytical uncertainty and minimum crystallization durations are calculated according to the method proposed by Klein and Eddy (2024). Emplacement ages are taken to be equivalent to the youngest zircon in each sample and are presented as  $\mu \pm x | y | z$ , where  $\mu$  is the calculated date,  $x$  is the uncertainty including only analytical uncertainties (including uncertainties related to the  $^{230}\text{Th}$  correction),  $y$  includes the uncertainty of the tracer calibration and  $z$  also includes the uncertainty on the decay constant (Condon et al. 2024).

### Re–Os geochronology

Petrography of the samples showed molybdenite crystals vary between 70 and 200  $\mu\text{m}$  in size. Eighteen samples, covering all vein types and their spatial distribution



within the CIC, were selected for dating. The preparation of molybdenite separates started with cutting the samples as close to the veins as possible and light crushing with a rock hammer (without contact with the metal) and sieving (< 5 mm). Molybdenite separation followed the bulk sample HF dissolution approach (Lawley and Selby 2012). The Re–Os analyses were performed in the Source Rock and Sulphide Geochronology and Geochemistry Laboratory, and Arthur Holmes Laboratory at Durham University (UK) following standard published protocols (e.g. Selby and Creaser 2001; Li et al. 2017). Specific procedural details are available in the supplementary material. Molybdenite dates were calculated using the  $^{187}\text{Re}$  decay constant of Smoliar et al. (1996) and are presented as:  $\mu \pm x | y$ , where  $\mu$  is the calculated date,  $x$  is the uncertainty including only analytical uncertainties, and  $y$  includes both analytical uncertainties and the uncertainty on the decay constant ( $2\sigma$  absolute level). Only analytical uncertainty is considered when computing the duration of the hydrothermal event(s) while all sources of systematic uncertainties are accounted for when comparing the Re–Os and U–Pb data.

## Results

### Zircon U–Pb geochronology

Most units contain varying proportions (0–13%) of rounded inherited or xenocrystic cores with two age populations, as detected by LA-ICP-MS U–Pb dating: one Triassic ( $199.8 \pm 6.1$  to  $245.8 \pm 5.6$ ) with a main population yielding a concordia date of  $221.0 \pm 0.6$  Ma ( $n = 49$ ,  $\text{MSWD} = 1.2$ ); and one early to mid-Eocene ( $40.22 \pm 1.67$  to  $53.90 \pm 2.63$ ). Overall, the proportion of such cores is the highest (> 6%) in samples from the northern side of the CIC older than 34.6 Ma (see below) compared to a lower proportion (mostly < 4%) in the southern and youngest (< 34.9 Ma) part of the CIC (see supplementary material). The cores often present a dark overgrowth at the interface with the oscillatory zoned Eocene overgrowth.

Two hundred and twenty individual zircon grains from 22 porphyry samples across the CIC were dated by CA-ID-TIMS (Fig. 4). Dates with high uncertainty were discarded ( $2\sigma > 1\%$  of the date; see details in the supplementary material). The U–Pb dates range over 3.3 Myr and show a complex, multi-million-year history of zircon crystallization. All porphyries present significant dispersion of single crystal dates, with nearly uninterrupted zircon crystallization dates spanning up to a million years within the same sample (Fig. 4).

### Chuquicamata mine

The Este Porphyry yields single crystal dates between  $34.402 \pm 0.034$  and  $35.451 \pm 0.096$  Ma, and all samples present a similar range of dates and similar distribution patterns (Fig. 4). One exception is for sample CQ2020 with a significantly narrower range of dates (ca. 0.15 Myr interval) and a very distinct distribution pattern. The youngest grains of all Este Porphyry samples range between  $34.402 \pm 0.034$  and  $34.751 \pm 0.162$  Ma.

Two samples mapped as the Oeste and Banco Porphyries yield dates akin to the Este Porphyry, with values between  $34.570 \pm 0.043$  and  $35.225 \pm 0.127$  Ma, and  $34.914 \pm 0.099$  and  $36.102 \pm 0.032$  Ma, respectively. In turn, other samples also mapped as Oeste and Banco Porphyries yield much younger single crystal dates between  $33.624 \pm 0.070$  and  $33.860 \pm 0.047$  Ma, and  $33.249 \pm 0.050$  and  $34.133 \pm 0.034$  Ma, respectively.

### Radomiro tomic

The zircon dates obtained for the Radomiro Tomic (RT), and Radomiro Tomic Norte (RTN) deposits tend to be systematically older than those obtained for the Chuquicamata mine. The Este Porphyry exhibits single crystal zircon dates ranging from  $34.605 \pm 0.039$  to  $35.877 \pm 0.026$  Ma yielding an overall duration of zircon crystallization of > 1 Myr. Notably, the southernmost Este sample from RT (RT2210, Fig. 1), located in the corridor that connects the two mines, yields zircon dates akin to the ones obtained in Chuquicamata and younger compared to the other samples in RT and RTN.

The samples of the Oeste, Fino and Banco porphyries in RT yield single crystal zircon date distributions similar to the Este Porphyry. The Oeste porphyry presents dates that range from  $34.886 \pm 0.055$  to  $36.583 \pm 0.025$  Ma, whereas the Banco porphyry yields dates varying between  $34.888 \pm 0.17$  to  $35.756 \pm 0.079$  Ma. One sample mapped as the Fino Porphyry follows the same pattern as the other porphyries, with dates between  $35.014 \pm 0.082$  and  $36.275 \pm 0.083$  Ma. However, a second sample also mapped as the Fino Porphyry, yields much younger dates ( $33.723 \pm 0.034$  to  $33.992 \pm 0.057$  Ma) and much shorter duration of zircon crystallization (minimum of 123 kyr).

In RTN, the Oeste porphyry yields much younger dates than the Este porphyry, ranging between  $33.880 \pm 0.036$  and  $34.175 \pm 0.025$  Ma and a minimum duration of zircon crystallization of 190 kyr.

### Zircon geochemistry

Zircon trace element data is consistent across all porphyries and mines of the CIC (Fig. 5). Most grains have very low Ti concentrations (4 to 1 ppm), Eu/Eu\* ratios between 0.35 and

**Fig. 4** Geochronologic summary for the CIC from CA-ID-TIMS U–Pb zircon and NTIMS Re–Os molybdenite chronology. We report <sup>230</sup>Th-corrected <sup>206</sup>Pb/<sup>238</sup>U dates for zircons, indicating the youngest single crystal date for each sample, and Re/Os dates for molybdenite. Porphyry samples are organized from North to South. The KDE plots in the bottom are weighted by the reverse uncertainty of each data point. <sup>40</sup>Ar/<sup>39</sup>Ar dates from Reynolds et al. (1998), Arnot (2003) and Barra et al (2013) were recalculated using updated age values for reference material and decay constant (see supplementary material) and include all sources of uncertainty

0.7, Hf contents around 1.2 wt.% and Yb/Dy ratios of 3–11. A slight positive correlation is observed between Th/U and Ti (Fig. 5a) whereas a negative trend is observed between Ti and both Hf and Yb/Dy (Fig. 5b, c).

No systematic change in composition is observed between cores, rims, and outer rims within sample. Within a single grain, it is common to observe a core to outer rim decrease in Ti content and Th/U ratio and an increase in Yb/Dy (Fig. 6). However, reverse zoning patterns are also locally observed. Finally, the trace element geochemistry of zircon is mostly independent of the date of the grain (Fig. 6), except for Th/U being slightly lower for the younger porphyries (Fig. 5a).

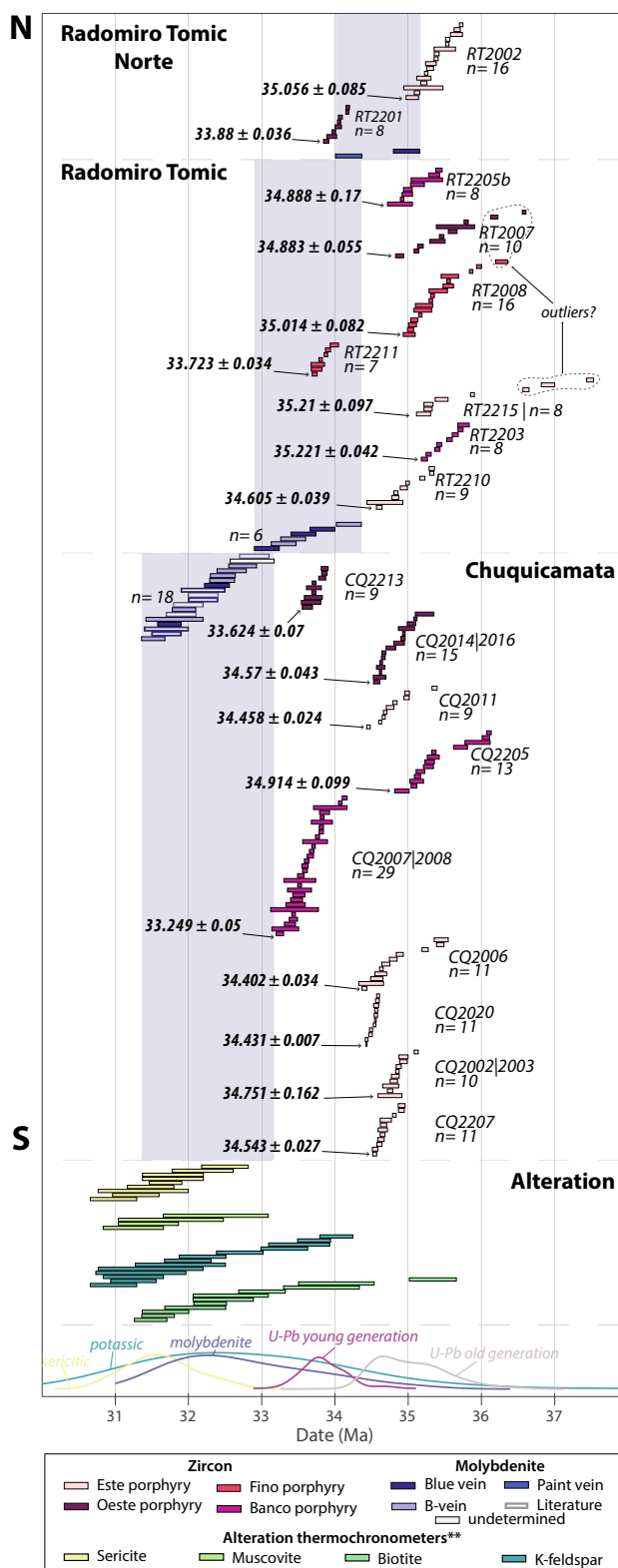
**Molybdenite geochronology**

Eighteen new Re–Os molybdenite dates are presented for the CIC (Fig. 4), which, when combined with previously published Re–Os dates, reveal a protracted duration of hydrothermal activity spanning up to 3.5 Myr. Within the Chuquicamata mine, the obtained Re–Os dates range from 31.52 ± 0.13 | 0.16 to 32.74 ± 0.16 | 0.19 Ma. A similarly long-lived Re–Os molybdenite date record is also observed in the RT mine. The dates range from 34.19 ± 0.14 | 0.18 and 33.07 ± 0.13 | 0.17 Ma. The northern part of the intrusive complex (RT Norte) yields two molybdenite dates of 34.98 ± 0.14 | 0.18 and 34.19 ± 0.15 | 0.18 Ma. No systematic relationship between date and vein type was observed in any of the deposits.

**Discussion**

**Nomenclature of the CIC porphyries**

Although the four mapped porphyries that make up the CIC are distinguished based on their textural characteristics and cross-cutting relationships (Fig. 2), they share the same composition, mineralogy, and zircon geochemistry (Fig. 5). Our new high-precision geochronology results reveal a previously unresolved level of complexity in the CIC and within individual porphyry units that requires rethinking the emplacement history of the CIC. Importantly, different samples, mapped as the same unit, yield



single zircon dates that vary by up to 1 Myr (e.g. Banco and Oeste porphyries in Chuquicamata; Fino and Banco porphyries in Radomiro Tomic; Fig. 4) with a group of samples consistently older than 34.5 Ma and one group

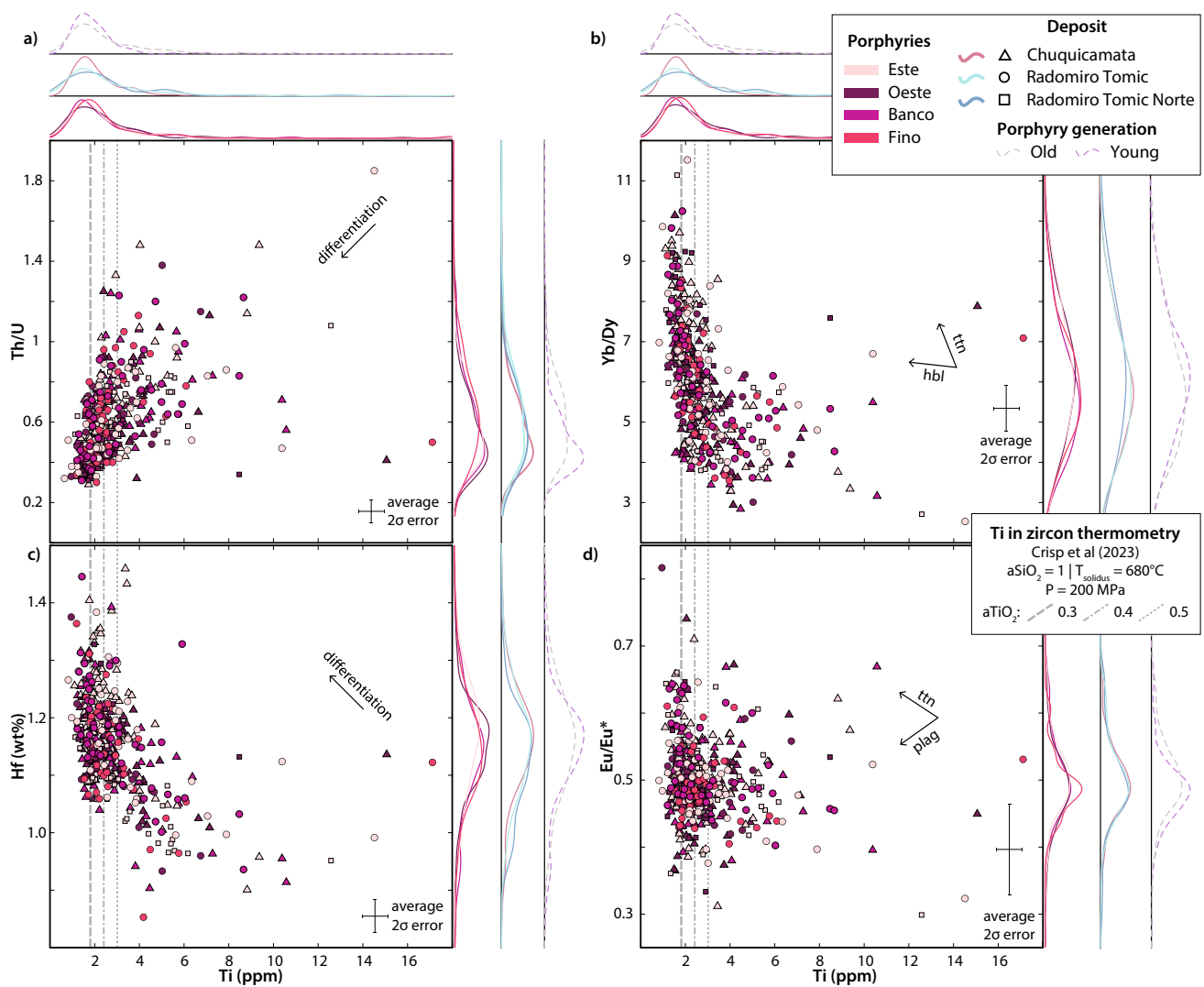


**Fig. 5** LA-ICP-MS zircon trace element composition of zircons from the CIC. Arrows show the trends compatible with an assemblage of zircon, apatite and titanite  $\pm$  hornblende. Vertical lines denote the cal-

culated Ti content for zircons crystallizing at the solidus temperature (680 °C for wet haplogranite composition, Johannes and Holtz 1996) with varying  $a_{\text{TiO}_2}$  (0.3–0.5), assuming 200 MPa (Crisp et al. 2023)

consistently younger than 34.0 Ma. Even though the textures observed within each unit agree with their nomenclature, the younger group of samples of the Banco, Oeste and Fino porphyries systematically present a slightly higher groundmass proportion (see supplementary material).

Given the chemical monotony of all the CIC porphyries, the occurrence of more than one generation of the same variety, even separated in time, seems reasonable if the main difference is only textural. Regardless of the reason, understanding the evolution of the CIC is independent of the names of the porphyries and from here forth, we will simply refer to the two distinct generations of porphyries as “young” (< 34 Ma) and “old” (> 34.5 Ma).

## Emplacement and evolution of the CIC

Our new petrochronological dataset on the CIC reveals its previously unrecognized complexity in stark contrast to its geochemical and mineralogical monotony. In essence, porphyry dykes and stocks are hypabyssal intrusions emplaced and quenched in the uppermost few kilometres of the crust (< 4 km, Sillitoe 2010) upon extrusion from a deeper located magma reservoir. Following this view, the spread of zircon dates within each sample (which can vary between 0.158 and 1.292 Myr in the CIC) provides a time-resolved window into the evolution of the magma reservoir. Following previous studies which applied high-precision geochronology to



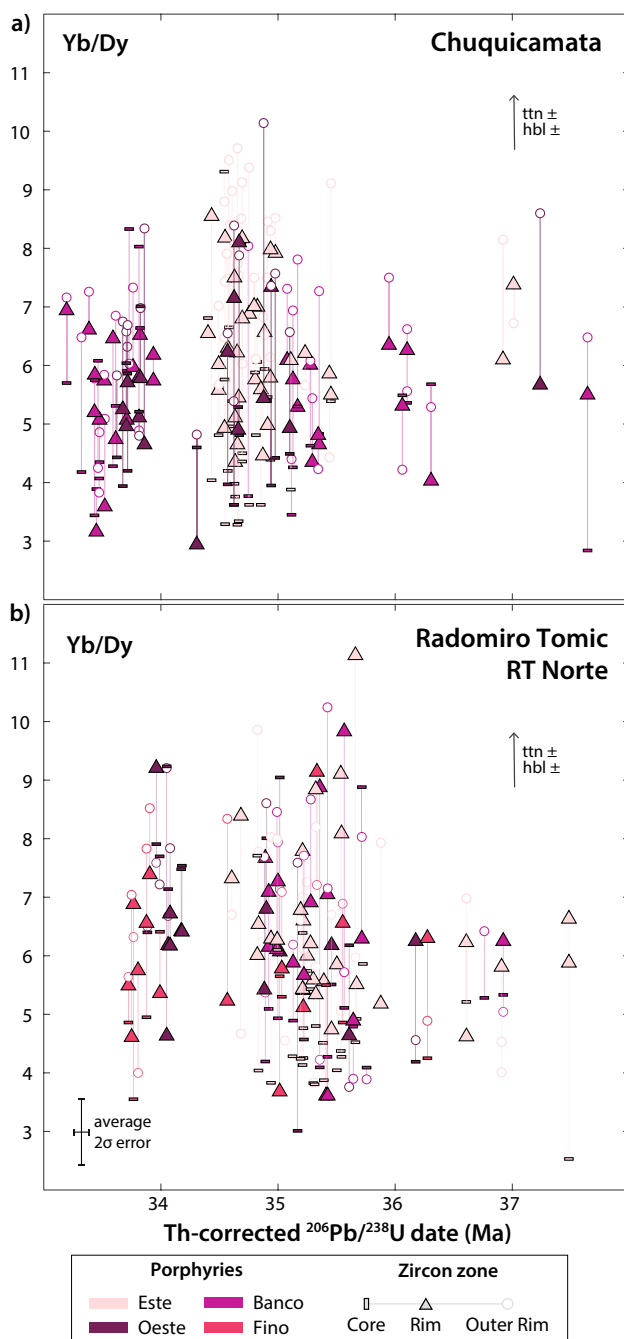


**Fig. 6** Relationship between zircon date and zircon trace element composition (Yb/Dy). Trace element composition was obtained in-situ on different zones of the crystal by LA-ICP-MS and U–Pb dates were obtained by CA-ID-TIMS on the same crystal. Arrows show the trends compatible with an assemblage of zircon, apatite and titanite ± hornblende. Note the overall composition is independent of zircon date. Normal zoning (increasing Yb/Dy from core to rim to outer rim) is observed in most grains, but reverse zoning is also present

porphyry dykes and stocks, we interpret the youngest date of each sample as the best approximation to its emplacement age (e.g. von Quadt et al. 2011; Chelle-Michou et al.

2014; Large et al. 2020, 2021; Markovic et al 2024), while the older dates record the evolution of the magma reservoir prior to emplacement.

Our new high-precision geochronological data show that much of the CIC, corresponding to the old porphyries, has been incrementally assembled between  $35.221 \pm 0.042 \mid 0.045 \mid 0.059$  ( $\pm x \mid y \mid z$  as detailed in Methods) and  $34.402 \pm 0.034 \mid 0.038 \mid 0.053$  Ma with systematically younger dates towards the south (between  $35.221 \pm 0.042 \mid 0.045 \mid 0.059$  and  $34.605 \pm 0.039 \mid 0.042 \mid 0.056$  Ma at RT + RTN, and between  $34.914 \pm 0.099 \mid 0.10 \mid 0.11$  and  $34.402 \pm 0.034 \mid 0.038 \mid 0.053$  Ma at Chuquicamata). Although cross-cutting relationships between texturally different porphyries could be observed (Fig. 2), it is likely that more cryptic contacts between similar-looking porphyries may have been obscured by the extensive hydrothermal alteration. It is noteworthy that the oldest dated porphyry at Chuquicamata was mapped as the Banco porphyry. Unfortunately, we did not date the contiguous Este porphyry within which it emplaced. This highlights that despite the extensive size of our dataset, our sampling remains affected by some degrees of undersampling making any duration a minimum estimate. In addition, although a single zircon crystal can record a protracted crystallization over 100's of kyr from core to rim (e.g. Tierney et al 2016, 2019), the dissolution and analysis of a bulk crystal using the CA-ID-TIMS methodology as applied in this study, thus could yield an average out of these internal differences and therefore also result in potentially shorter computed durations.

Following a ca. 522 kyr apparent hiatus in zircon crystallization (between  $34.402 \pm 0.034$  Ma in CQ2006 and  $33.880 \pm 0.036$  Ma in RT2201), porphyry emplacement resumed with the young porphyries throughout the CIC. Our data also highlight a clear younging trend from  $33.880 \pm 0.036 \mid 0.040 \mid 0.054$  Ma in RTN to  $33.249 \pm 0.050 \mid 0.052 \mid 0.063$  Ma in the southern limb of Chuquicamata.

Most zircons in the CIC contain very low Ti contents ( $\sim 2$  to 3 ppm). Based on the Ti-in-zircon thermometer, assuming  $a\text{SiO}_2$  of 1,  $a\text{TiO}_2$  between 0.3 and 0.5, and a pressure of 200 MPa (Crisp et al. 2023), these concentrations correspond to temperature nearing the wet granite solidus (680 °C; Johannes and Holtz 1996). Although  $a\text{TiO}_2$  mostly influences the computed temperature, it is a dynamic parameter that remains difficult to constrain (Fonseca Teixeira et al. 2023) and higher values than those assumed would result in unreasonable subsolidus temperatures. Zircon Hf concentration, Th/U, Yb/Dy and the Eu anomaly, all of which trace magmatic differentiation (e.g. Wotzlaw et al. 2013; Buret et al. 2016; Large et al. 2018; Nathwani et al. 2021), show similar values across the CIC. Zircon trace element stratigraphy, from core to rim to outer rim, most often shows that decreasing Ti concentrations are commonly linked to decreasing Th/U and increasing Yb/Dy and Hf content

(Figs. 5, 6). These trends are compatible with co-crystallization of zircon, apatite and titanite  $\pm$  hornblende with decreasing temperature. However, some grains also show partial reverse zoning patterns likely pointing to recharge events. It is noteworthy that no correlation exists between trace element zoning and zircon dates (Fig. 6). The petrochronological data suggest the existence of an overall homogenous near-solidus magma reservoir that has been kept thermally and chemically buffered for at least 2.2 Myr in the case of the old porphyries and 1.0 Myr for the young porphyries.

### The magmatic-hydrothermal history of the CIC

At the sample scale, molybdenite dominantly predates both the main stage of copper mineralization and the late quartz-sericite-pyrite veins (Fig. 3; Ossandón et al. 2001; Faunes et al. 2005; Rivera et al. 2012; Skarmeta 2021). Deposit-scale patterns also show that the quartz-molybdenite mineralization follows the main stage quartz-sericite alteration which is also linked to the main stage copper mineralization. This suggests that at any given place in the CIC, molybdenite precipitates prior to Cu sulphides but molybdenite Re–Os dates closely approximate the timing of Cu precipitation. Our new molybdenite Re–Os data, combined with published dates (Barra et al. 2013; Zentilli et al. 2021), shows a total timespan of  $\sim$ 3.5 Myr of hydrothermal activity and that the dates become systematically younger towards the south of the CIC.

The initiation of CIC porphyry emplacement is recorded in the RT and RTN areas just before 35 Ma. Only in the northernmost part, porphyry emplacement is coeval with a small Cu–Mo mineralization event at  $34.98 \pm 0.14 \mid 0.18$  Ma (Fig. 7a, e). The incremental building of the bulk of the CIC megadyke follows for  $819 \pm 54$  kyr ( $35.221 \pm 0.042$  in RT2203 and  $34.402 \pm 0.034$  in CQ2006), across the whole extent of the complex, with the last intrusion being recorded within the Chuquicamata mine (Fig. 7b, e).

The main mineralization event likely started at RTN and RT around 34.19 Ma, coeval to the emplacement of the young porphyries, and lasts for about  $1.12 \pm 0.19$  Myr in this part of the CIC (Fig. 7c). In Chuquicamata, the mineralization starts at  $32.74 \pm 0.16$  Ma, shortly postdating the emplacement of the young porphyries, and lasts for  $1.38 \pm 0.26$  Myr without any known associated porphyry emplacement (Fig. 7d, e). It is noteworthy that the Re–Os molybdenite dates are continuous between RT and Chuquicamata. This further confirms that the two deposits derive from continuous outgassing of the same underlying magma reservoir.

In Chuquicamata, the absence of young porphyries that are synchronous with the beginning of mineralization could reflect undersampling. Indeed, small porphyry dikes, neglected or not accessible during the sampling campaigns,

could well be coeval with the beginning of the mineralization, or additional molybdenite dating could also extend towards older dates coeval with the dated young porphyries. Previous  $^{40}\text{Ar}/^{39}\text{Ar}$  dates obtained for alteration minerals were recalculated using updated values for reference materials and decay constants (see supplementary material). These dates mostly agree with the molybdenite dates obtained here and even slightly extend the alteration event to both older and younger dates, with a large overlap between the timing of the potassic and sericitic alteration assemblages (data from Reynolds et al. 1998; Arnott 2003; Barra et al. 2013). Apart from a suspiciously old date from a chloritized biotite aliquot, the oldest  $^{40}\text{Ar}/^{39}\text{Ar}$  dates perfectly overlap with the age of the young porphyry, supporting the genetic link between the young porphyry and the hydrothermal alteration and mineralization event.

The lack of porphyry emplacement over the million-year duration of the hydrothermal event show that outgassing of the magma reservoir can persist long after the emplacement of the last (outcropping) porphyries. Numerical models suggest that such a feature is consistent with moderate to high magma intrusion rate ( $> 0.001$  km<sup>3</sup>/yr; Chelle-Michou et al. 2017).

Both the age of emplacement of the old and the young porphyries with their associated hydrothermal activity show a general southward younging trend along the ca. 12 km N–S axis of the complex that was sampled. Previous structural investigations highlighted that the emplacement of the CIC and the related hydrothermal activity occurred during a dextral transtensional regime controlled by the proto-West fault and the Mesabi Fault (Lindsay et al. 1995; Tomlinson et al. 2018; Rojas-Arancibia 2023), followed by rapid exhumation (McInnes et al. 1999). As both magma emplacement and hydrothermal fluid circulation are facilitated by structural anisotropies in the crust (Tosdal and Richards 2001; Codeço et al. 2022), we speculate that the general southward younging trends may be the result of a “channelling” process caused by the transtensional regime.

### Volume, duration, and thermal constraints on porphyry-forming magma reservoirs

The duration of zircon crystallization obtained by high precision U–Pb geochronology can provide a time-resolved window into the underlying magma system that fed upper crustal reservoirs, whether the magmatic reservoir becomes erupted material, a batholith, or porphyry intrusions. For the CIC, our results show an overall zircon crystallization record of at least  $2.181 \pm 0.042$  Myr for the old porphyries and  $0.951 \pm 0.077$  Myr for the young porphyries.

It is commonly understood that the parental magmas of porphyry copper deposits are not especially enriched in Cu (Cline and Bodnar 1991; Chelle-Michou et al. 2017; Zhang

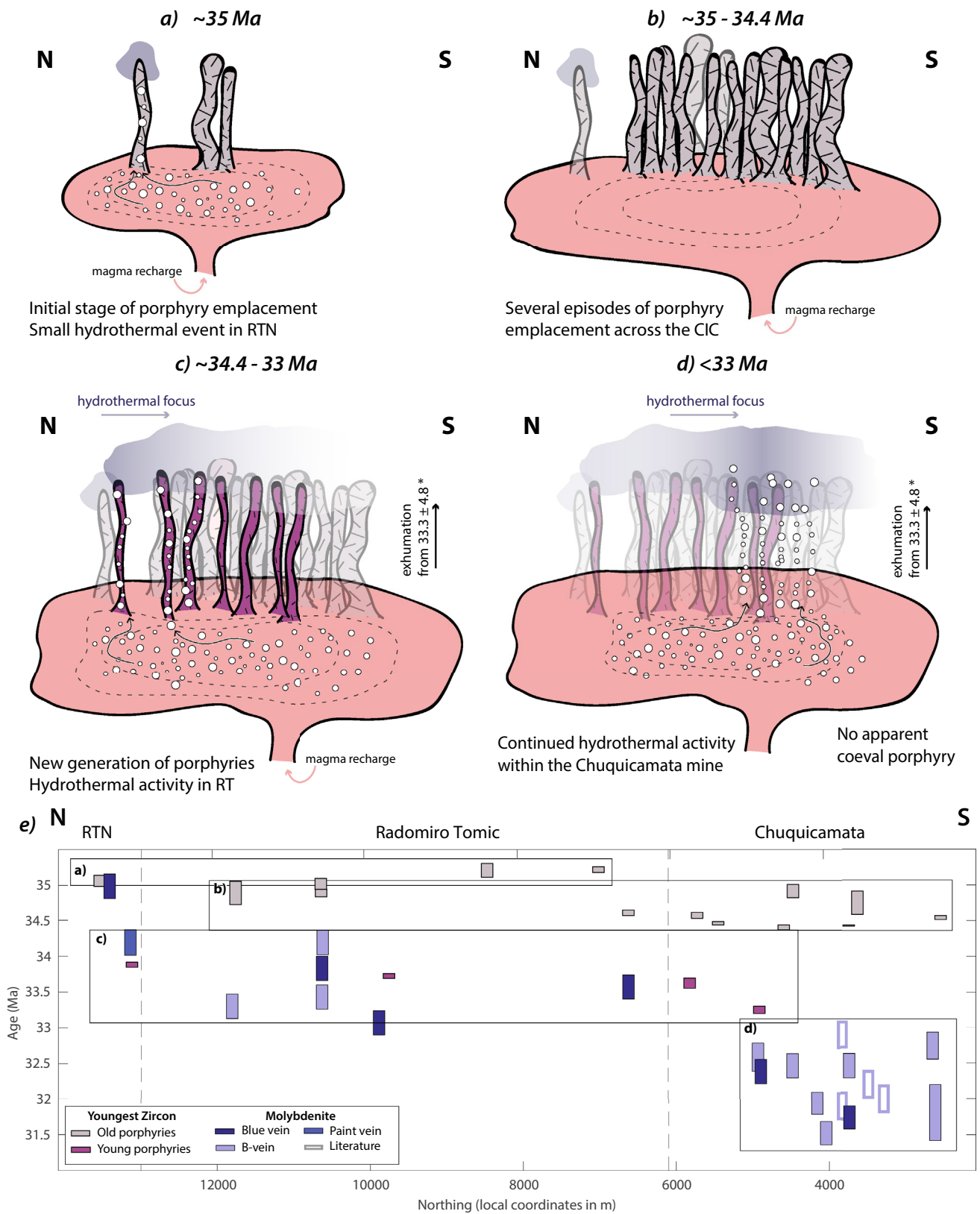


**Fig. 7** Sketch for the proposed magmatic-hydrothermal evolution of the CIC (not to scale). Different colours for dykes represent different generations of porphyries. **e** Geochronology summary with emplacement

date (youngest zircon) for different samples and molybdenite dates. \*Apatite fission track data from McInnes et al (1999) suggest exhumation from at least  $33.3 \pm 4.8$  Ma



and Audétat 2017). Hence, mass balance calculations show that very large volumes of magma are required to source enough Cu to form large porphyry copper deposits. Assuming an initial Cu content of 30 ppm in the parental magma of the CIC, a minimum volume of 1,800 km<sup>3</sup> of magma is necessary to source the 136.6 Mt of Cu contained in the Chuquicamata and Radomiro Tomic deposits. This result assumes a 100% efficiency of Cu precipitation and only represents the minimum volume associated with young porphyries. No constraints can be used to estimate the size of the reservoir that sourced the old porphyries, suggesting the real volume of magma involved in the formation of the CIC can be even larger, possibly on the order of 10,000 km<sup>3</sup>. Considering these numbers and the timescale provided by the U–Pb zircon record, a time-averaged magma accumulation rate on the order of 0.002 km<sup>3</sup>/yr is estimated for the CIC magmatism. Although such values correspond to the world median pluton-filling rates (Menand et al. 2015), the associated volumes are akin to those of the largest eruptions of monotonous intermediate ignimbrites.

Monotonous intermediate ignimbrites and the CIC share some characteristics such as high crystallinity, chemical homogeneity, large volumes of parent magma reservoir and long-lived magmatic activity in the upper crust. The Altiplano Puna Volcanic Complex (APVC) erupted 15,000 km<sup>3</sup> of magma in numerous episodes between 10 and 1 Ma, following a flare-up event at around 10 Ma (de Silva 1989; de Silva et al. 2006). In one of the main ignimbrite sources of the APVC, the Pastos Grandes Caldera Complex, a long-lived chemically and thermally buffered upper crustal magma reservoir has been proposed to explain the 1.1 Myr period of (nearly) continuous zircon crystallization of the system (Kaiser et al. 2017). Other volcanic centers in the Altiplano complex record at least 400 kyr of zircon crystallization prior to eruption (Kern et al. 2016). Despite the similarities, there is no evidence of coeval volcanism associated with the CIC. Volcanic activity is often understood to hinder the formation of porphyry deposits, due to the catastrophic loss of volatiles and metals (Pasteris 1996; Sillitoe 2010; Buret et al. 2017). In fact, supergiant to behemothian porphyry copper deposits have been suggested to be “failed eruptions” (Pasteris 1996; Large et al. 2021; Chiaradia and Caricchi 2022) due to the similarities they share with large eruptions.

Such similarities warrant a discussion of how such gigantic magma reservoir grow without triggering eruptions. The thermal maturation of the crust is an important factor in the context of the monotonous intermediate ignimbrites, as shown by numerical simulations (e.g. de Silva and Gregg 2014; Karakas et al. 2017) and observed in the Altiplano Puna (Kaiser et al. 2017). Similarly, the occurrence of significant precursor magmatism in the context of a porphyry copper system has also been pointed to as a possible factor

facilitating the formation of large magma reservoirs associated with these deposits (Chelle-Michou and Rottier 2021). In the CIC, important precursor magmatism includes not only the old generation of porphyries but also the Los Picos and Fortuna igneous complexes (45 to 42 Ma and 40 to 37 Ma, respectively; Tomlinson et al. 2018 and references therein). Altogether, the area has been magmatically active over more than 10 Myr which provides favorable conditions for a thermally mature crust at the time of the emplacement of the CIC, thereby creating an upper crustal rheology that helped circumvent large eruptions that otherwise would have hindered the formation of the Cu deposits by venting magmatic volatiles. This evolution resembles the post-caldera evolution of the APVC (at around 75–100 ka) which is characterized by the eruption of relatively small (collectively ca. 40 km<sup>3</sup>), texturally mature, and chemically monotonous domes sourced from magma reservoirs combining a volume of > 3000 km<sup>3</sup> (Tierney et al. 2016). The evolution of the APVC from a cataclysmic eruption regime to a dominantly intrusive regime (with minor domes) has been linked to a significant decrease magma recharge rate (Tierney et al. 2016). We also note that the volume of the CIC and of its plutonic root compares well with those estimated for the APVC domes and of their source magma reservoirs, respectively, further suggesting a similar evolution of the two magmatic systems.

### Implications for supergiant porphyry copper systems

Numerical models and existing high-precision geochronological data suggest a first order correlation between the size of the deposit (contained mass of Cu), the volume of ore-forming magma and the durations of the magmatic-hydrothermal activity; from a few thousand years for deposits containing a few million tons of Cu to timescales of 1 Myr for deposits containing 100 Mt of Cu (e.g. Chelle-Michou et al. 2017; Chelle-Michou and Rottier 2021; Chiaradia and Caricchi 2022; see Fig. 8).

In the case where both a pre-mineral ore-forming porphyry and a post-mineral intrusion have been dated, the maximum duration of the hydrothermal event, bracketed by the magmatic ages, is indicated (Fig. 8). Despite possible inaccuracies, weighted mean dates (for SHRIMP or LA-ICP-MS U–Pb data) are presented in the same figure for the Los Bronces and El Teniente deposits, two of the largest porphyry copper deposits in the world, with 140 and 112 Mt of contained copper, respectively (resources + past production, Camus and Castelli 2021; Codelco 2022).

Our new high-precision geochronological data for the CIC align well with what would be expected for such behemothian deposits (Fig. 8; e.g. Chelle-Michou et al. 2017; Chelle-Michou and Rottier 2021). Smaller deposits (a few

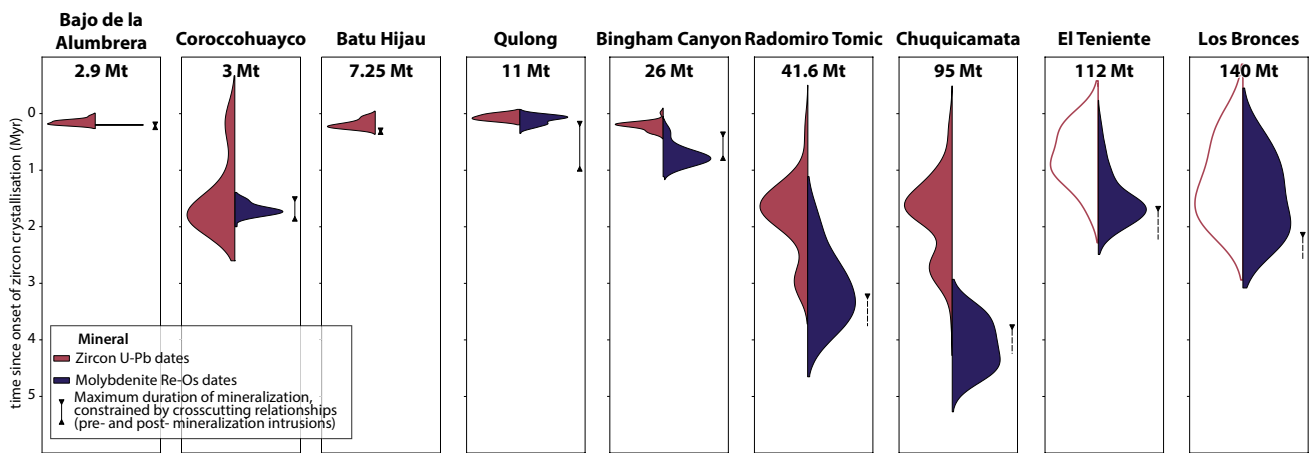


**Fig. 8** Timescales of ore-forming magmatic and hydrothermal activities for several deposits, based on compilation of zircon U–Pb CA-ID-TIMS (except for El Teniente and Los Bronces, which are LA-ICP-MS and SHRIMP data) and, whenever possible, molybdenite Re–Os

N-TIMS results. Whenever available, zircon bracketing by crosscutting relationships is also presented. References and details on how durations were calculated are presented in the supplementary material

Mt of contained Cu) have relatively short and overlapping (ca. < 10 to 100 kyr) ore-forming magmatic and hydrothermal activities (Fig. 8). As the deposits get larger, the overall duration of ore-forming magmatic activity does not change significantly, but the timescale of the hydrothermal activity gets longer and may last up to 1 Myr after the onset of zircon crystallization. In the Chuquicamata district, the deposits record a much longer magmatic history (lasting up to 3 Myr after the onset of zircon crystallization) and the hydrothermal activity not only lasts longer (up to 3.5 Myr) but also continues even after the end of known magmatic activity (Fig. 8). Our results confirm that the correlation between duration of mineralization and metal endowment of a deposit is also valid in the context of behemothian deposits.

### Continuous vs pulsed hydrothermal activity

The seemingly continuous molybdenite record of the CIC suggests a similarly continuous mineralization duration. This contrasts with some suggestions that supergiant deposits may result from the superimposition of distinct short-lived events of few tens of thousands of years or less (e.g., Li et al. 2017; Large et al. 2020). For example, for the Qulong deposit (11 Mt of contained Cu), Li et al. (2017) obtained a total interval of  $266 \pm 13$  kyr of discontinuous mineralization with at least two short-lived events of  $38 \pm 11$  and  $59 \pm 10$  kyr, separated by a gap of  $48 \pm 10$  kyr. In the El Teniente deposit (112 Mt of contained Cu), five short-lived magmatic-hydrothermal pulses over a period of almost 2 Myr, separated by periods of quiescence of 100–300 kyr are documented (Maksaev et al. 2004). Whereas a longer duration of the main mineralizing pulse (up to 580 kyr) is considered to be associated with a composite intrusion, formed by several spatially

overlapping dykes (Spencer et al. 2015). Yet, both studies may equally suffer from some degree of undersampling such that it remains unclear whether the apparent temporal gaps are true geological features or sampling artefacts.

On the other hand, numerical models of magma emplacement in the upper crust highlight that such systems outgas continuously, possibly at varying rates (e.g. Parmigiani et al. 2017; Chelle-Michou et al. 2017; Lamy-Chappuis et al. 2020). Upon fluid focussing in the apical part of magma reservoirs, the fluid pressure episodically reaches the failure criterion and dynamic permeability modelling highlights the existence of rapidly ascending ( $\ll 1$  kyr) permeability-overpressure waves (e.g. Weis et al. 2012; Weis 2014). These models highlight that while magmatic fluid can be continuously outgassed, thermomechanical feedback occurring within the fluid plume region can be responsible for short-lived pulses of which duration is unresolvable with geochronological methods. Ultimately, the question can be reformulated as whether giant to behemothian porphyry-system pulsate at high ( $\ll 1$  kyr timescale) or low (10–100 kyr timescale) frequency.

To address this question, we computed the copper precipitation rate for a range of porphyry deposits with well constrained hydrothermal timescales and copper tonnage (Fig. 9; see supplementary material for details on the calculations and timescale estimates). In the investigated deposits, rates range between  $0.025 \pm 0.001$  and more than 0.1 Mt/kyr. As a comparison the atmospheric Cu flux measured from high-temperature ( $> 400$  °C) fumaroles at the White Island andesitic volcano, New Zealand, reached up to 0.3 Mt/kyr (Le Cloarec et al. 1992). For the smaller deposits (e.g. Bajo de la Alumbraera, Corocchohuayco) the duration of mineralization is only a maximum value which allows

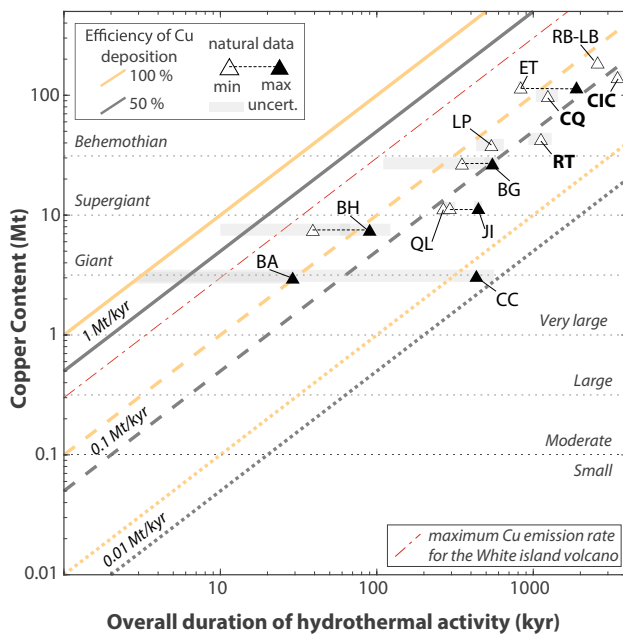


**Fig. 9** Results of the simulation showing the relationship between duration of hydrothermal activity and Cu endowment. BA Bajo de la Alumbrera, CC Corocohuayco, BH Batu Hijau, QL Qulong, JI Jiama, BG Bingham Canyon, LP Los Pelambres, ET El Teniente, RB-LB Rio Blanco-Los Bonces, RT Radomiro Tomic, CQ Chuquicamata, CIC Chuquicamata Intrusive Complex (includes CQ, RT and RTN). References and details on how durations were calculated are presented in the supplementary material

for significantly shorter durations, and proportionally higher copper deposition rates. From a theoretical standpoint, the fluid Cu flux directly depends on the volumetric cooling rate of the outgassing magma reservoir. Numerical simulations of magma outgassing highlight that even at high magma intrusion rate of  $0.01 \text{ km}^3/\text{yr}$ , and initial magmatic Cu concentrations of 50 ppm the maximum copper flux remains below  $1 \text{ Mt/kyr}$  (Chelle-Michou et al. 2017). This puts an upper constraint on the permissible Cu deposition rate associated with porphyry deposits.

This analysis shows that although compiled porphyry deposits cover three orders of magnitude of Cu endowment, their Cu deposition rate only varies by a factor of four. Ultimately, this suggests that the frequency of copper depositional pulses is similar across the range of size of porphyry deposits. This frequency is more likely high than low, making Cu deposition virtually continuous rather than pulsed.

## Conclusions

Here, timescales of magmatic and hydrothermal activity in the Chuquicamata Intrusive Complex (CIC) were investigated using zircon and molybdenite high-precision geochronology. Zircon petrochronology reveals a previously

unrecognized, highly complex evolution for the CIC, with a magma reservoir that remained chemically and thermally buffered for over 3 Myr, producing at least two main events of porphyry emplacement. The younger generation of porphyry, commonly occurring as small metric to decametric bodies, is the one temporally linked to the onset of the mineralizing event across the district which lasted a total of 3.5 Myr. In the CIC, both the magmatic and hydrothermal activities migrate southward over time, which we tentatively attribute to the coeval activity of the transtensional proto-West Fault and Mesabi fault system.

Our results provide unprecedented evidence that behemothian porphyry copper deposits require large volumes of magma ( $> 1000 \text{ km}^3$ ), and million-year-long timescales of magmatic and hydrothermal activities. We show that the rate of copper precipitation varies little in nature and is independent on the size of the deposit, defining the duration of hydrothermal activity as an overarching control on the final copper endowment of a deposit. Therefore, quantifying the magmatic-hydrothermal timescales in the early stages of exploration should improve chances of finding new behemothian deposits.

Finally, we highlight that the parental magma reservoirs that feed behemothian porphyry copper systems share similarities with monotonous intermediate ignimbrites and that such porphyry systems can provide insights to understanding the evolution of large upper to mid crustal magma reservoirs and their ability to erupt catastrophically or to continuously crystallize and degas.

**Supplementary Information** The online version contains supplementary material available at <https://doi.org/10.1007/s00410-024-02167-4>.

**Acknowledgements** ALV and CCM acknowledge funding from ETH Zürich. We are immensely grateful to the members of CODELCO, especially Elizabeth Demané, Giorgio Realini, Renato Valdéz Romo, Silvino Córdova, Claudio Rojas, Augusto Mont, Gabriel Leiva, Rafael González and Rubén Pardo for providing valuable insights into the geology of the Chuquicamata District, and for providing access to the mine, drill core samples and granting permission to publish this study. We thank Marcel Guillong, Peter Tolan and Lorenzo Tavazzani for the help with LA-ICP-MS analysis, and Dawid Szymanowski and Chetan Nathwani for insightful discussions. DS acknowledges Chris Ottley and Geoff Nowell for laboratory support. We thank Axel Schmitt and David Chew for constructive feedback that helped improve this manuscript.

**Funding** Open access funding provided by Swiss Federal Institute of Technology Zurich. Eidgenössische Technische Hochschule Zürich.

**Data availability** All data is provided in the supplementary material.

## Declarations

**Conflict of interest** The authors have no competing interests to declare that are relevant to the content of this article.

**Open Access** This article is licensed under a Creative Commons Attribution 4.0 International License, which permits use, sharing,



adaptation, distribution and reproduction in any medium or format, as long as you give appropriate credit to the original author(s) and the source, provide a link to the Creative Commons licence, and indicate if changes were made. The images or other third party material in this article are included in the article's Creative Commons licence, unless indicated otherwise in a credit line to the material. If material is not included in the article's Creative Commons licence and your intended use is not permitted by statutory regulation or exceeds the permitted use, you will need to obtain permission directly from the copyright holder. To view a copy of this licence, visit <http://creativecommons.org/licenses/by/4.0/>.

## References

- Amilibia A, Sàbat F, McClay KR et al (2008) The role of inherited tectono-sedimentary architecture in the development of the central Andean mountain belt: Insights from the Cordillera de Domeyko. *J Struct Geol* 30:1520–1539. <https://doi.org/10.1016/j.jsg.2008.08.005>
- Annen C (2009) From plutons to magma chambers: Thermal constraints on the accumulation of eruptible silicic magma in the upper crust. *Earth Planet Sci Lett* 284:409–416. <https://doi.org/10.1016/j.epsl.2009.05.006>
- Arnott AM (2003) Evolution of the hydrothermal alteration at the Chuquicamata porphyry copper system, Northern Chile. PhD, Dalhousie University
- Ballard JR, Palin JM, Williams IS et al (2001) Two ages of porphyry intrusion resolved for the super-giant Chuquicamata copper deposit of northern Chile by ELA-ICP-MS and SHRIMP. *Geol* 29:383. [https://doi.org/10.1130/0091-7613\(2001\)029%3c0383:TAOPIR%3e2.0.CO;2](https://doi.org/10.1130/0091-7613(2001)029%3c0383:TAOPIR%3e2.0.CO;2)
- Barra F, Alcota H, Rivera S et al (2013) Timing and formation of porphyry Cu–Mo mineralization in the Chuquicamata district, northern Chile: new constraints from the Toki cluster. *Miner Depos* 48:629–651. <https://doi.org/10.1007/s00126-012-0452-1>
- Baumgartner R, Fontboté L, Spikings R et al (2009) Bracketing the age of magmatic-hydrothermal activity at the Cerro de Pasco epithermal polymetallic deposit, Central Peru: a U–Pb and  $^{40}\text{Ar}/^{39}\text{Ar}$  study. *Econ Geol* 104:479–504. <https://doi.org/10.2113/gsecongeo.104.4.479>
- Buret Y, von Quadt A, Heinrich C et al (2016) From a long-lived upper-crustal magma chamber to rapid porphyry copper emplacement: reading the geochemistry of zircon crystals at Bajo de la Alumbrera (NW Argentina). *Earth Planet Sci Lett* 450:120–131. <https://doi.org/10.1016/j.epsl.2016.06.017>
- Buret Y, Wotzlav J-F, Roozen S et al (2017) Zircon petrochronological evidence for a plutonic-volcanic connection in porphyry copper deposits. *Geology* 45:623–626. <https://doi.org/10.1130/G38994.1>
- Campbell IH, Ballard JR, Palin JM et al (2006) U–Pb zircon geochronology of granitic rocks from the Chuquicamata-El Abra Porphyry Copper Belt of Northern Chile: excimer laser ablation ICP-MS analysis. *Econ Geol* 101:1327–1344. <https://doi.org/10.2113/gsecongeo.101.7.1327>
- Camus F, Castelli JC (2021) Historia, Exploración y Geología de los Yacimientos Metalíferos de Chile 900-2021. Origo Ediciones, Santiago
- Camus F, Dilles JH (2001) A special issue devoted to porphyry copper deposits of Northern Chile preface. *Econ Geol*. <https://doi.org/10.2113/gsecongeo.96.2.233>
- Chelle-Michou C, Rottier B (2021) Transcrustal magmatic controls on the size of porphyry Cu systems: state of knowledge and open questions. *Tectonomagmatic influences on metallogeny and hydrothermal ore deposits: a tribute to Jeremy P. Richards*, vol I. Society of Economic Geologists, pp 87–100
- Chelle-Michou C, Schaltegger U (2023) U–Pb dating of mineral deposits: from age constraints to ore-forming processes. In: Huston D, Gutzmer J (eds) *Isotopes in economic geology, metallogenesis and exploration*. Springer International Publishing, Cham, pp 37–87
- Chelle-Michou C, Chiaradia M, Ovtcharova M et al (2014) Zircon petrochronology reveals the temporal link between porphyry systems and the magmatic evolution of their hidden plutonic roots (the Eocene Corocochuayco deposit, Peru). *Lithos* 198–199:129–140. <https://doi.org/10.1016/j.lithos.2014.03.017>
- Chelle-Michou C, Rottier B, Caricchi L, Simpson G (2017) Tempo of magma degassing and the genesis of porphyry copper deposits. *Sci Rep* 7:40566. <https://doi.org/10.1038/srep40566>
- Chiaradia M, Caricchi L (2022) Supergiant porphyry copper deposits are failed large eruptions. *Commun Earth Environ* 3:1–9. <https://doi.org/10.1038/s43247-022-00440-7>
- Chiaradia M, Schaltegger U, Spikings R et al (2013) How accurately can we date the duration of magmatic-hydrothermal events in porphyry systems? An invited paper. *Econ Geol* 108:565–584. <https://doi.org/10.2113/econgeo.108.4.565>
- Clark AH (1993) Are outsize porphyry copper deposits either anatomically or environmentally distinctive? In: Whiting BH, Hodgson CJ, Mason R (eds) *Giant ore deposits*. Society of Economic Geologists
- Cline JS, Bodnar RJ (1991) Can economic porphyry copper mineralization be generated by a typical calc-alkaline melt? *J Geophys Res: Solid Earth* 96:8113–8126. <https://doi.org/10.1029/91JB00053>
- Cobbold PR, Rossello EA, Roperch P et al (2007) Distribution, timing, and causes of Andean deformation across South America. *Geol Soc, Lond Spec Publ* 272:321–343. <https://doi.org/10.1144/GSL.SP.2007.272.01.17>
- Codeço MS, Weis P, Andersen C (2022) Numerical modeling of structurally controlled ore formation in magmatic-hydrothermal systems. *Geochem, Geophys, Geosyst* 23:e2021GC010302. <https://doi.org/10.1029/2021GC010302>
- Codelco (2022) Comprehensive Report. CODELCO
- Condon D, Schoene B, Schmitz M et al (2024) Recommendations for the reporting and interpretation of isotope dilution U–Pb geochronological information. *GSA Bull*. <https://doi.org/10.1130/B37321.1>
- Crisp LJ, Berry AJ, Burnham AD et al (2023) The Ti-in-zircon thermometer revised: the effect of pressure on the Ti site in zircon. *Geochim Cosmochim Acta*. <https://doi.org/10.1016/j.gca.2023.04.031>
- de Silva SL (1989) Altiplano-Puna volcanic complex of the central Andes. *Geology* 17:1102–1106. [https://doi.org/10.1130/0091-7613\(1989\)017%3c1102:APVCOT%3e2.3.CO;2](https://doi.org/10.1130/0091-7613(1989)017%3c1102:APVCOT%3e2.3.CO;2)
- de Silva SL, Gregg PM (2014) Thermomechanical feedbacks in magmatic systems: Implications for growth, longevity, and evolution of large caldera-forming magma reservoirs and their supereruptions. *J Volcanol Geoth Res* 282:77–91. <https://doi.org/10.1016/j.jvolgeores.2014.06.001>
- de Silva S, Zandt G, Trumbull R et al (2006) Large ignimbrite eruptions and volcano-tectonic depressions in the Central Andes: a thermomechanical perspective. *Geol Soc, Lond, Spec Publ* 269:47–63. <https://doi.org/10.1144/GSL.SP.2006.269.01.04>
- Deckart K, Clark AH, Cuadra P, Fanning M (2013) Refinement of the time-space evolution of the giant Mio-Pliocene Río Blanco-Los Bronces porphyry Cu–Mo cluster, Central Chile: new U–Pb (SHRIMP II) and Re–Os geochronology and  $^{40}\text{Ar}/^{39}\text{Ar}$  thermochronology data. *Miner Depos* 48:57–79. <https://doi.org/10.1007/s00126-012-0412-9>
- Faunes A, Hinze F, Siña A et al (2005) Chuquicamata core of a planetary scale Cu–Mo anomaly. In: Porter TM (ed) *Super porphyry*

- copper and gold deposits: a global perspective, vol 1. PGC Publishing, Adelaide, pp 151–174
- Fonseca Teixeira LM, Troch J, Bachmann O (2023) The dynamic nature of aTiO<sub>2</sub>: Implications for Ti-based thermometers in magmatic systems. *Geology*. <https://doi.org/10.1130/G51587.1>
- Guillong M, von Quadt A, Sakata S et al (2014) LA-ICP-MS Pb–U dating of young zircons from the Kos–Nisyros volcanic centre, SE Aegean arc. *J Anal at Spectrom* 29:963–970. <https://doi.org/10.1039/C4JA00009A>
- Guillong M, Sliwinski JT, Schmitt A et al (2016) U–Th zircon dating by laser ablation single collector inductively coupled plasma-mass spectrometry (LA-ICP-MS). *Geostand Geoanal Res* 40:377–387. <https://doi.org/10.1111/j.1751-908X.2016.00396.x>
- Harrison TM, McDougall I (1981) Excess <sup>40</sup>Ar in metamorphic rocks from Broken Hill, New South Wales: implications for <sup>40</sup>Ar/<sup>39</sup>Ar age spectra and the thermal history of the region. *Earth Planet Sci Lett* 55:123–149. [https://doi.org/10.1016/0012-821X\(81\)90092-3](https://doi.org/10.1016/0012-821X(81)90092-3)
- Johannes W, Holtz F (1996) *Petrogenesis and experimental petrology of granitic rocks*. Springer, Berlin Heidelberg
- Jowitt SM, Mudd GM, Thompson JFH (2020) Future availability of non-renewable metal resources and the influence of environmental, social, and governance conflicts on metal production. *Commun Earth Environ* 1:1–8. <https://doi.org/10.1038/s43247-020-0011-0>
- Kaiser JF, De Silva S, Schmitt AK et al (2017) Million-year melt–presence in monotonous intermediate magma for a volcanic–plutonic assemblage in the Central Andes: contrasting histories of crystal-rich and crystal-poor super-sized silicic magmas. *Earth Planet Sci Lett* 457:73–86. <https://doi.org/10.1016/j.epsl.2016.09.048>
- Karakas O, Degruyter W, Bachmann O, Dufek J (2017) Lifetime and size of shallow magma bodies controlled by crustal-scale magmatism. *Nature Geosci* 10:446–450. <https://doi.org/10.1038/ngeo2959>
- Kent AJR, Cooper KM (2017) How well do zircons record the thermal evolution of magmatic systems? *Geology* 46:111–114. <https://doi.org/10.1130/G39690.1>
- Kern JM, de Silva SL, Schmitt AK et al (2016) Geochronological imaging of an episodically constructed subvolcanic batholith: U–Pb in zircon chronochemistry of the Altiplano-Puna Volcanic Complex of the Central Andes. *Geosphere* 12:1054–1077. <https://doi.org/10.1130/GES01258.1>
- Klein BZ, Eddy MP (2024) What’s in an age? Calculation and interpretation of ages and durations from U–Pb zircon geochronology of igneous rocks. *GSA Bull* 4:7. <https://doi.org/10.1130/B36686.1>
- Lamy-Chappuis B, Heinrich CA, Driesner T, Weis P (2020) Mechanisms and patterns of magmatic fluid transport in cooling hydrous intrusions. *Earth Planet Sci Lett* 535:116111. <https://doi.org/10.1016/j.epsl.2020.116111>
- Large SJE, Quadt AV, Wotzlaw J-F et al (2018) Magma evolution leading to porphyry Au–Cu Mineralization at the Ok Tedi Deposit, Papua New Guinea: trace element geochemistry and high-precision geochronology of igneous zircon. *Econ Geol* 113:39–61. <https://doi.org/10.5382/econgeo.2018.4543>
- Large SJE, Wotzlaw J-F, Guillong M et al (2020) Resolving the timescales of magmatic and hydrothermal processes associated with porphyry deposit formation using zircon U–Pb petrochronology. *Geochronology* 2:209–230. <https://doi.org/10.5194/gchron-2-209-2020>
- Large SJE, Buret Y, Wotzlaw JF et al (2021) Copper-mineralised porphyries sample the evolution of a large-volume silicic magma reservoir from rapid assembly to solidification. *Earth Planet Sci Lett* 563:116877. <https://doi.org/10.1016/j.epsl.2021.116877>
- Lawley CJM, Selby D (2012) Re–Os Geochronology of quartz-enclosed ultrafine molybdenite: implications for ore geochronology. *Econ Geol* 107:1499–1505. <https://doi.org/10.2113/econgeo.107.7.1499>
- Le Cloarec MF, Allard P, Ardouin B et al (1992) Radioactive isotopes and trace elements in gaseous emissions from White Island, New Zealand. *Earth Planet Sci Lett* 108:19–28. [https://doi.org/10.1016/0012-821X\(92\)90057-3](https://doi.org/10.1016/0012-821X(92)90057-3)
- Li Y, Selby D, Condon D, Tapster S (2017) Cyclic magmatic-hydrothermal evolution in porphyry systems: high-precision U–Pb and Re–Os geochronology constraints on the Tibetan Qulong porphyry Cu–Mo deposit. *Econ Geol* 112:1419–1440. <https://doi.org/10.5382/econgeo.2017.4515>
- Lindsay DD, Zentilli M, Rivera JRDL (1995) Evolution of an active ductile to brittle shear system controlling mineralization at the Chuquicamata Porphyry Copper Deposit, Northern Chile. *Int Geol Rev* 37:945–958. <https://doi.org/10.1080/00206819509465434>
- Maksaev V, Zentilli M (1988) Marco metalogénico regional de los megadepósitos de tipo pórfido cuprífero del Norte Grande de Chile. *Congreso Geológico Chileno*. Vol. 1. No. 5
- Maksaev V, Zentilli M (1999) Fission track thermochronology of the Domeyko Cordillera, northern Chile; implications for Andean tectonics and porphyry copper metallogenesis. *Explor Min Geol* 8:65–89
- Maksaev V, Munizaga F, McWilliams M et al (2004) New chronology for El Teniente, Chilean Andes, from U–Pb, <sup>40</sup>Ar/<sup>39</sup>Ar, Re–Os, and fission-track dating: implications for the evolution of a supergiant porphyry Cu–Mo deposit. In: Sillitoe RH, Perelló J, Vidal CE (eds) *Andean metallogeny: new discoveries, concepts, and updates*. Society of Economic Geologists. <https://doi.org/10.5382/SP.11>
- Mamani M, Worner G, Sempere T (2010) Geochemical variations in igneous rocks of the Central Andean orocline (13° S to 18° S): tracing crustal thickening and magma generation through time and space. *Geol Soc Am Bull* 122:162–182. <https://doi.org/10.1130/B26538.1>
- Markovic S, Brunner M, Müller L et al (2024) Zircon petrochronology of Au-rich porphyry and epithermal deposits in the Golden Quadrilateral (Apuseni Mountains, Romania). *Econ Geol* 119:967–988. <https://doi.org/10.5382/econgeo.5073>
- McInnes BIA, Farley KA, Sillitoe RH, Kohn BP (1999) Application of apatite (U–Th)/He thermochronometry to the determination of the sense and amount of vertical fault displacement at the Chuquicamata porphyry copper deposit, Chile. *Econ Geol* 94:937–947. <https://doi.org/10.2113/gsecongeo.94.6.937>
- Menand T, Annen C, de Saint BM (2015) Rates of magma transfer in the crust: Insights into magma reservoir recharge and pluton growth. *Geology* 43:199–202. <https://doi.org/10.1130/G36224.1>
- Mpodozis C, Cornejo P (2012) Cenozoic tectonics and porphyry copper systems of the Chilean Andes. *Geology and genesis of major copper deposits and districts of the world: a tribute to Richard H. Sillitoe*. Society of Economic Geologists
- Mudd GM, Weng Z, Jowitt SM (2013) A detailed assessment of global Cu resource trends and endowments. *Econ Geol* 108:1163–1183. <https://doi.org/10.2113/econgeo.108.5.1163>
- Nathwani CL, Simmons AT, Large SJE et al (2021) From long-lived batholith construction to giant porphyry copper deposit formation: petrological and zircon chemical evolution of the Quellaveco District, Southern Peru. *Contrib Mineral Petrol* 176:12. <https://doi.org/10.1007/s00410-020-01766-1>
- Onstott TC, Mueller C, Vrolijk PJ, Pevear DR (1997) Laser <sup>40</sup>Ar/<sup>39</sup>Ar microprobe analyses of fine-grained illite. *Geochim Cosmochim Acta* 61:3851–3861. [https://doi.org/10.1016/S0016-7037\(97\)00288-3](https://doi.org/10.1016/S0016-7037(97)00288-3)

- Ossandón G, Fréaut CR, Gustafson LB et al (2001) Geology of the Chuquicamata mine: a progress report. *Econ Geol* 96:249–270. <https://doi.org/10.2113/gsecongeo.96.2.249>
- Parmigiani A, Degruyter W, Leclaire S et al (2017) The mechanics of shallow magma reservoir outgassing. *Geochem Geophys Geosyst* 18:2887–2905. <https://doi.org/10.1002/2017GC006912>
- Pasteris JD (1996) Mount Pinatubo volcano and “negative” porphyry copper deposits. *Geology* 24:1075–1078. [https://doi.org/10.1130/0091-7613\(1996\)024%3c1075:MPVANP%3e2.3.CO;2](https://doi.org/10.1130/0091-7613(1996)024%3c1075:MPVANP%3e2.3.CO;2)
- Reynolds P, Ravenhurst C, Zentilli M, Lindsay D (1998) High-precision  $^{40}\text{Ar}/^{39}\text{Ar}$  dating of two consecutive hydrothermal events in the Chuquicamata porphyry copper system, Chile. *Chem Geol* 148:45–60. [https://doi.org/10.1016/S0009-2541\(97\)00129-0](https://doi.org/10.1016/S0009-2541(97)00129-0)
- Richards JP (2013) Giant ore deposits formed by optimal alignments and combinations of geological processes. *Nat Geosci* 6:911–916. <https://doi.org/10.1038/ngeo1920>
- Rivera SL, Alcota H, Proffett J et al (2012) Update of the geologic setting and porphyry Cu–Mo deposits of the Chuquicamata District, Northern Chile. *Geology and genesis of major copper deposits and districts of the world: a tribute to Richard H. Sillitoe*
- Rojas-Arancibia R (2023) Propuesta de Modelo y Evolución Estructural del Yacimiento Radomiro Tomic, Distrito Chuquicamata. XVI Congreso Geológico Chileno, Santiago
- Schaltegger U, Ovtcharova M, P. Gaynor S, et al (2021) Long-term repeatability and interlaboratory reproducibility of high-precision ID-TIMS U–Pb geochronology. *J Anal at Spectrom* 36:1466–1477. <https://doi.org/10.1039/D1JA00116G>
- Schoene B, Baxter EF (2017) Petrochronology and TIMS. *Rev Miner Geochem* 83:231–260. <https://doi.org/10.2138/rmg.2017.83.8>
- Selby D, Creaser RA (2001) Re–Os geochronology and systematics in molybdenite from the endako porphyry molybdenum deposit, British Columbia, Canada. *Econ Geol* 96:197–204. <https://doi.org/10.2113/gsecongeo.96.1.197>
- Sillitoe RH (2010) Porphyry copper systems. *Econ Geol* 105:3–41. <https://doi.org/10.2113/gsecongeo.105.1.3>
- Singer DA., Berger VI, Moring BC (2008) Porphyry copper deposits of the world: Database and grade and tonnage models, 2008 (No. 2008–1155). US Geological Survey
- Skarmeta J (2021) Structural controls on alteration stages at the Chuquicamata Copper–Molybdenum deposit, Northern Chile. *Econ Geol* 116:1–28. <https://doi.org/10.5382/econgeo.4769>
- Smoliar MI, Walker RJ, Morgan JW (1996) Re–Os ages of group IIA, IIIA, IVA, and IVB iron meteorites. *Science* 271:1099–1102. <https://doi.org/10.1126/science.271.5252.1099>
- Spencer ET, Wilkinson JJ, Creaser RA, Seguel J (2015) The distribution and timing of molybdenite mineralization at the El Teniente Cu–Mo porphyry deposit, Chile. *Econ Geol* 110:387–421. <https://doi.org/10.2113/econgeo.110.2.387>
- Tierney CR, Schmitt AK, Lovera OM, de Silva SL (2016) Voluminous plutonism during volcanic quiescence revealed by thermochemical modeling of zircon. *Geology* 44:683–686. <https://doi.org/10.1130/G37968.1>
- Tierney CR, Reid MR, Vazquez JA, Chesner CA (2019) Diverse late-stage crystallization and storage conditions in melt domains from the Youngest Toba Tuff revealed by age and compositional heterogeneity in the last increment of accessory phase growth. *Contrib Miner Petrol* 174:31. <https://doi.org/10.1007/s00410-019-1566-6>
- Tomlinson AJ, Blanco N, Dilles JH, et al. (2018) Carta Calama, Región de Antofagasta, Servicio Nacional de Geología y Minería, Carta Geológica de Chile, Serie Geología Básica 199: 345 p., 1 mapa escala 1:100.000. Santiago.
- Tosdal RM, Richards JP (2001) Magmatic and structural controls on the development of porphyry Cu  $\pm$  Mo  $\pm$  Au deposits. In: Richards JP, Tosdal RM (eds) Structural controls on ore genesis. Society of Economic Geologists
- von Quadt A, Erni M, Martinek K et al (2011) Zircon crystallization and the lifetimes of ore-forming magmatic-hydrothermal systems. *Geology* 39:731–734. <https://doi.org/10.1130/G31966.1>
- von Quadt A, Wotzlaw J-F, Buret Y et al (2016) High-precision zircon U/Pb geochronology by ID-TIMS using new  $10^{13} \Omega$  resistors. *J Anal at Spectrom* 31:658–665. <https://doi.org/10.1039/C5JA00457H>
- Weis P (2014) The Physical hydrology of ore-forming magmatic-hydrothermal systems. In: Kelley KD, Golden HC (eds) Building exploration capability for the 21st century. Society of Economic Geologists
- Weis P, Driesner T, Heinrich CA (2012) Porphyry-copper ore shells form at stable pressure-temperature fronts within dynamic fluid plumes. *Science* 338:1613–1616. <https://doi.org/10.1126/science.1225009>
- Wotzlaw J-F, Schaltegger U, Frick DA et al (2013) Tracking the evolution of large-volume silicic magma reservoirs from assembly to supereruption. *Geology* 41:867–870. <https://doi.org/10.1130/G34366.1>
- Wotzlaw J-F, Buret Y, Large SJE et al (2017) ID-TIMS U–Pb geochronology at the 0.1‰ level using  $10^{13} \Omega$  resistors and simultaneous U and  $^{18}\text{O}/^{16}\text{O}$  isotope ratio determination for accurate  $\text{UO}_2$  interference correction. *J Anal at Spectrom* 32:579–586. <https://doi.org/10.1039/C6JA00278A>
- Zentilli M, Graves MC, Mathur R et al (2021) Locating the “Missing Half” of the giant Chuquicamata porphyry copper deposit, Chile. In: Sholeh A, Wang R (eds) Tectonomagmatic influences on metallogeny and hydrothermal ore deposits: a tribute to Jeremy P. Richards, vol I. Society of Economic Geologists
- Zhang D, Audétat A (2017) What caused the formation of the giant Bingham canyon porphyry Cu–Mo–Au Deposit? Insights from melt inclusions and magmatic sulfides. *Econ Geol* 112:221–244. <https://doi.org/10.2113/econgeo.112.2.221>

**Publisher's Note** Springer Nature remains neutral with regard to jurisdictional claims in published maps and institutional affiliations.